Metallogenesis and Formation of the Maliping Pb-Zn Deposit in Northeastern Yunnan: Constraints from H-O Isotopes, Fluid Inclusions, and Trace Elements

Yongsheng Yao [1], Hongsheng Gong [1,2,*], Runsheng Han [1,2,*], Changqing Zhang [3], Peng Wu [1,2] and Gang Chen [1]

[1] Faculty of Land Resources Engineering, Kunming University of Science and Technology, Kunming 650093, China; yaoyongsheng2021@163.com (Y.Y.); wupeng8104@163.com (P.W.); chengang@kust.edu.cn (G.C.)
[2] Southwest Institute of Geological Survey, Geological Survey Center for Non-Ferrous Metals Resources, Kunming 650093, China
[3] MNR Key Laboratory of Metallogeny and Mineral Assessment, Institute of Mineral Resources, Chinese Academy of Geological Sciences, Beijing 100037, China; zcqchangqing@163.com
* Correspondence: ghs7633@163.com (H.G.); 11301124@kust.edu.cn (R.H.); Tel.: +86-139-0886-1618 (H.G.)

Abstract: The Maliping large-scale Pb-Zn deposit is located in the Sichuan-Yunnan-Guizhou Pb-Zn polymetallic metallogenic triangle area (SYGT), where the Pb-Zn ore body is hosted in the interlayer fracture zone at the interface between siliceous cataclastic dolomite and clastic rocks in the Lower Cambrian Yuhucun Formation and is tectonically driven. Unlike other Pb-Zn deposits hosted in the Sinian and Carboniferous carbonate rocks in the area, the metallogenic mechanism and deep and peripheral ore prospecting prediction research require further exploration. In this study, representative samples of a typical orebody profile were systematically collected, and microthermometry of fluid inclusions and H-O isotopes and metal sulfide trace element analyses were performed. The main findings were as follows: (1) The fluid inclusion study showed that the ore-forming fluids have vapor-rich phase reduction characteristics of medium-low temperature, salinity, and density. (2) H-O isotopic studies showed that the ore-forming fluids are derived from the mixing of deep-source fluids flowing through the deep fold basement (Kunyang Group) and organic containing basin brine. (3) Rare earth element (REE) characteristics indicate that the ore-forming materials were primarily derived from the folded basement (Kunyang Group). (4) The trace element study showed that sphalerite is relatively enriched in Cu, Cd, Ga, and Ge, while depleted in Fe, Mn, Sn, and Co, similar to the typical Huize-type (HZT) Pb-Zn deposit in the area. Therefore, it is suitable to explore the deposit using a large-scale "four step style" ore prospecting method for ore prospecting and prediction. Moreover, the results provide a reference for the study of Pb-Zn metallogenic systems and new ideas for the deep and peripheral prospecting of Pb-Zn deposits in this area.

Keywords: H-O isotopes; fluid inclusions; trace elements; ore-forming materials sources; metallogenic mechanism; Maliping Pb-Zn deposit; Sichuan-Yunnan-Guizhou Pb-Zn polymetallic metallogenic triangle area

1. Introduction

The Sichuan-Yunnan-Guizhou Pb-Zn polymetallic metallogenic triangle area (SYGT) is situated on the southwestern margin of the Yangtze Block (Figure 1a) and is an important component of the large low-temperature metallogenic domains in southwest China [1–3]. The SYGT is the largest Pb-Zn metallogenic area in China, with over 500 Pb-Zn deposits (spots) distributed in the area [4,5]. These are controlled by fault structures and distributed in a beaded shape along larger-scale fault zones. Most deposits exhibit an average Pb + Zn grade exceeding 15% [6] and are rich in valuable elements, such as Ag and Ge [7–12]. In recent years, a large number of geologists have conducted research and development studies on Pb-Zn deposits in the area, but insufficient reserves in old mines and the

challenges of deep ore prospecting remain issues. Therefore, there is an urgent need to innovate and improve the metallogenic theory and ore prospecting methods and to identify deep replacement resources.

The ore body of the Maliping Pb-Zn deposit is a large-scale Pb-Zn deposit newly discovered in northeast Yunnan. It is hosted in the Lower Cambrian Yuhucun Formation (to facilitate comparison with previous research results, the stratigraphic division in this study still follows the original stratigraphic criteria), within the interlayer fracture zone of the interface between siliceous cataclastic dolomite and clastic rocks (Yunnan Nonferrous Geological, Geophysical, and Geochemical Exploration Survey, 2011 internal data). Although numerous studies have been conducted on carbonate-hosted Pb-Zn deposits in the SYGT, relatively few investigations have been conducted on Pb-Zn deposits hosted in the interlayer fracture zone of the interface between the siliceous cataclastic dolomite and clastic rocks. Previous studies have examined the genesis of the Maliping Pb-Zn deposit from different perspectives and proposed varying views: (1) Based on field geological characteristics and analysis of major and trace elements in the ore, Shen et al. [13] and He et al. [14] suggested that the deposit was based on the original ore layer formed by hydrothermal deposition and was driven and transformed mineralization by the eruption of the later Emeishan basalt, which had a submarine (volcanic) hydrothermal exhalative sedimentation + later (hydrothermal) superimposed transformation genesis. (2) Luo et al. [15] and Hu et al. [16] suggested that the deposit was of the Mississippi Valley type (MVT) through the study of dispersed elements in ore minerals and C-O-S-Pb isotopes. Luo et al. [17] suggested that the major metal source of the Maliping deposit was Proterozoic basement rocks (e.g., the Kunyang Group), whereas Early Cambrian black shales and phosphate rocks acted as secondary sources. The previous understanding of the genesis of the deposit remains controversial, and the research on the metallogenic mechanism and ore prospecting prediction of Pb-Zn deposits hosted in the interlayer fracture zone at the interface between siliceous cataclastic dolomite and clastic rock needs to be in-depth.

In this study, we performed microthermometry of fluid inclusions, microscopic laser Raman spectroscopy, H-O isotopic composition analysis, metal sulfide trace element analysis, and electron probe micro-analysis (EMPA)-mapping analysis to trace the characteristics and sources of ore-forming fluids in the Maliping Pb-Zn deposit. In addition, we conducted a comparative analysis with typical Pb-Zn deposits in the area to determine the genesis of the deposit and propose a metallogenic mechanism. These findings offer a new basis for the study of the regional Pb-Zn mineralization system and the ore prospecting prediction of deep and peripheral parts of the deposit.
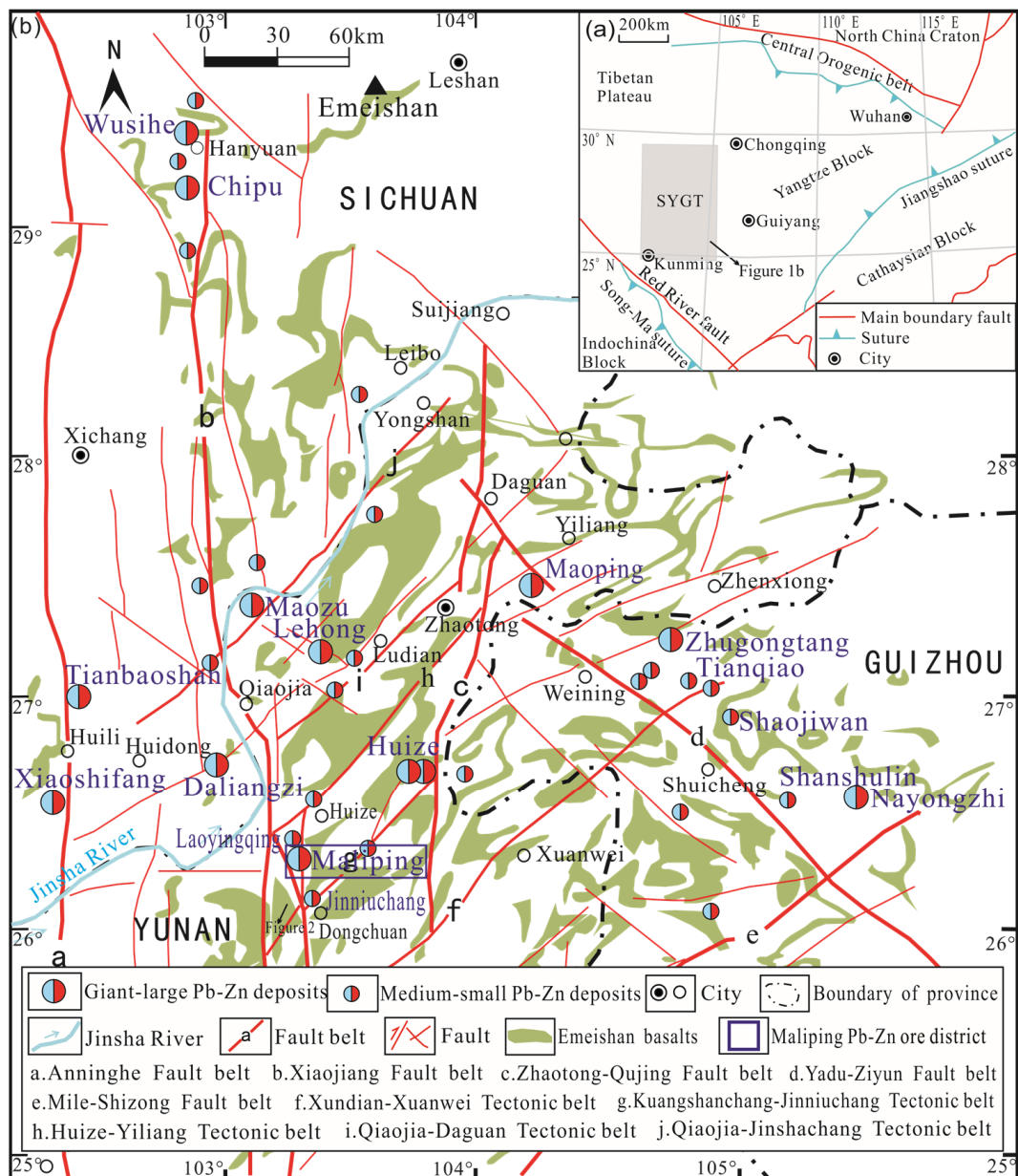
Figure 1. (**a**) Simplified tectonic map of southwest China [18]; (**b**) Distribution map of main faults and deposits in the SYGT [18].

2. Metallogenic Geological Background

The SYGT is located on the southwestern margin of the Yangtze Block (Figure 1a) and is controlled by three deep boundary faults: the NW-trending Yadu-Ziyun (Kangding-Yiliang-Shuicheng), NE-trending Mile-Shizong, and the NS-trending Anninghe fault belts (Figure 1b). The strata in the area mainly include basement and sedimentary cover, with an angular unconformity between them. Since the Archean, multiple stages of tectonic evolutions have occurred in the area, with the crystalline basement constituted by the Paleoproterozoic Kangding Group and the folded basement constituted by the Mesoproterozoic Kunyang and Huili groups [6,19].

The ore concentration area of northeastern Yunnan has formed eight NE-trending "Xi-type" tectonic mineralization belts from south to north (sinistral oblique thrust strike-slip fault-fold belt, controlling the spatial distribution of Pb-Zn deposits in the region), which are typical structures in the area [20,21]. The Maliping Pb-Zn deposit is located on

the eastern side of the Xiaojiang fault belt in northeastern Yunnan and is controlled by an interlayer fault on the eastern wing of the Wuxing anticline. Within the ore district, there is a monoclinic structure, developing NW- and nearly NS-trending faults. The NE-trending bedding fault was the main ore-controlling and ore-bearing fault. The strata in the ore district are distributed in a nearly NS-trending manner, trending eastward and exposing the Kunyang Group, Heishantou Formation, Sinian, Cambrian, Devonian, Carboniferous, Permian, and Quaternary (Figure 2a). No magmatic rock outcrops are observed in the ore district (Figure 2b).
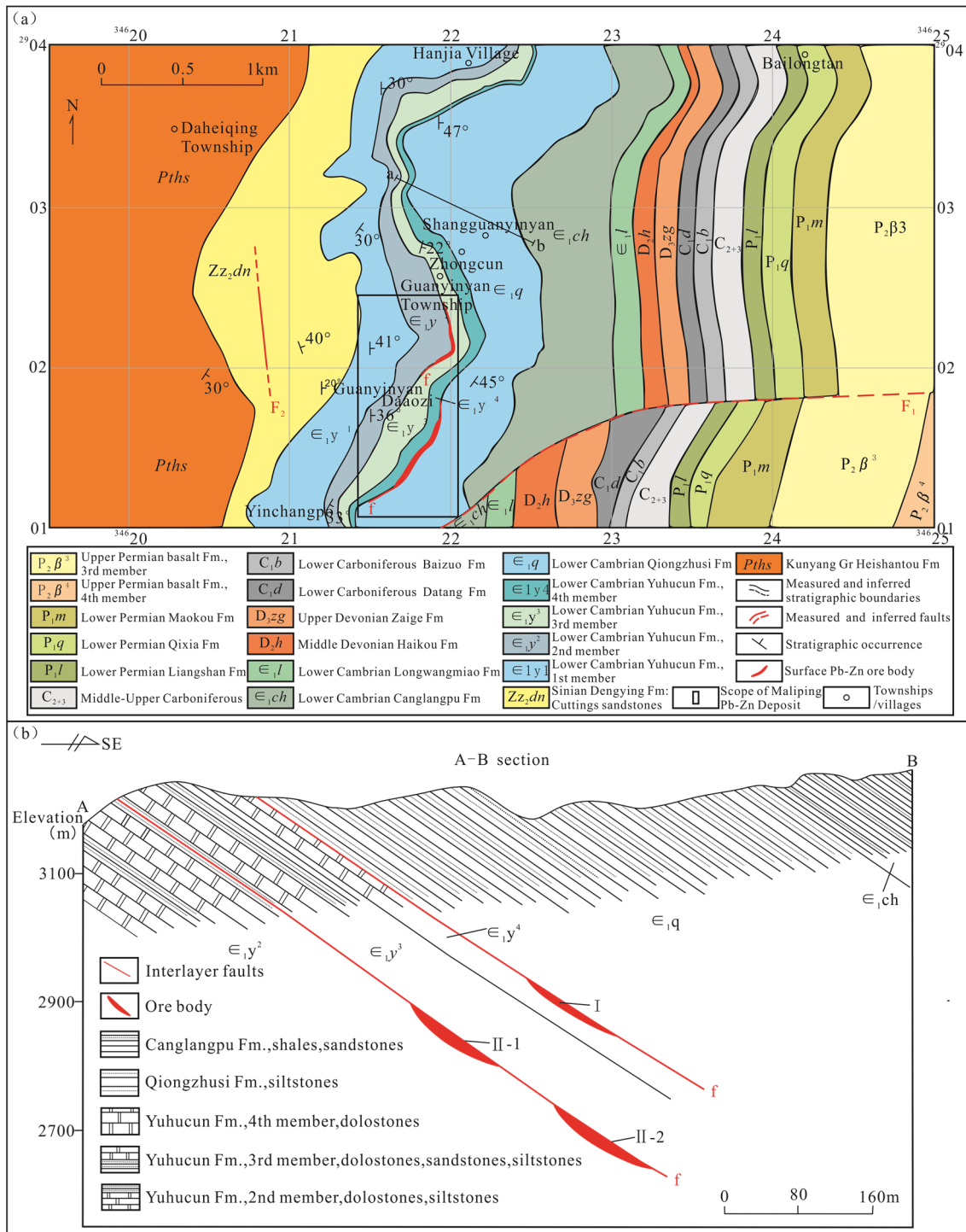

Figure 2. (**a**) Geological sketch map of the Maliping Pb-Zn deposit; (**b**) Geological section map of the Maliping Pb-Zn Deposit [16].

The ore bodies (I, II-1, and II-2) are hosted in the NEE-trending interlayer fracture zone at the interface between the siliceous cataclastic dolomite and clastic rocks in the Lower Cambrian Yuhucun Formation; however, a small portion also occurs along the NW-trending fault (Figure 3a,b), which is lenticular and stratoid (Figure 3b). The ore body strikes 68–156° and dips 15–42°, with an average true thickness of 1.63–2.69 m and an average Pb + Zn grade of 12.69%–15.89% (Yunnan Nonferrous Geological, Geophysical, and Geochemical Exploration Survey, 2011 internal data). The ore minerals are primarily sphalerite and galena, followed by pyrite and limonite; gangue minerals are mainly quartz. The ore textures are granular, mosaic, and porphyritic. The ore structure is primarily disseminated and brecciated but also includes banded, taxitic, veinlet, and laminated structures (Figure 3c,d). Pyrite and sphalerite are symbiotic (Figure 3e,g), galena metasomatic pyrite and sphalerite, quartz metasomatic galena, sphalerite, and pyrite (Figure 3e,f,h,i). Wall-rock alteration is primarily characterized by silicification.
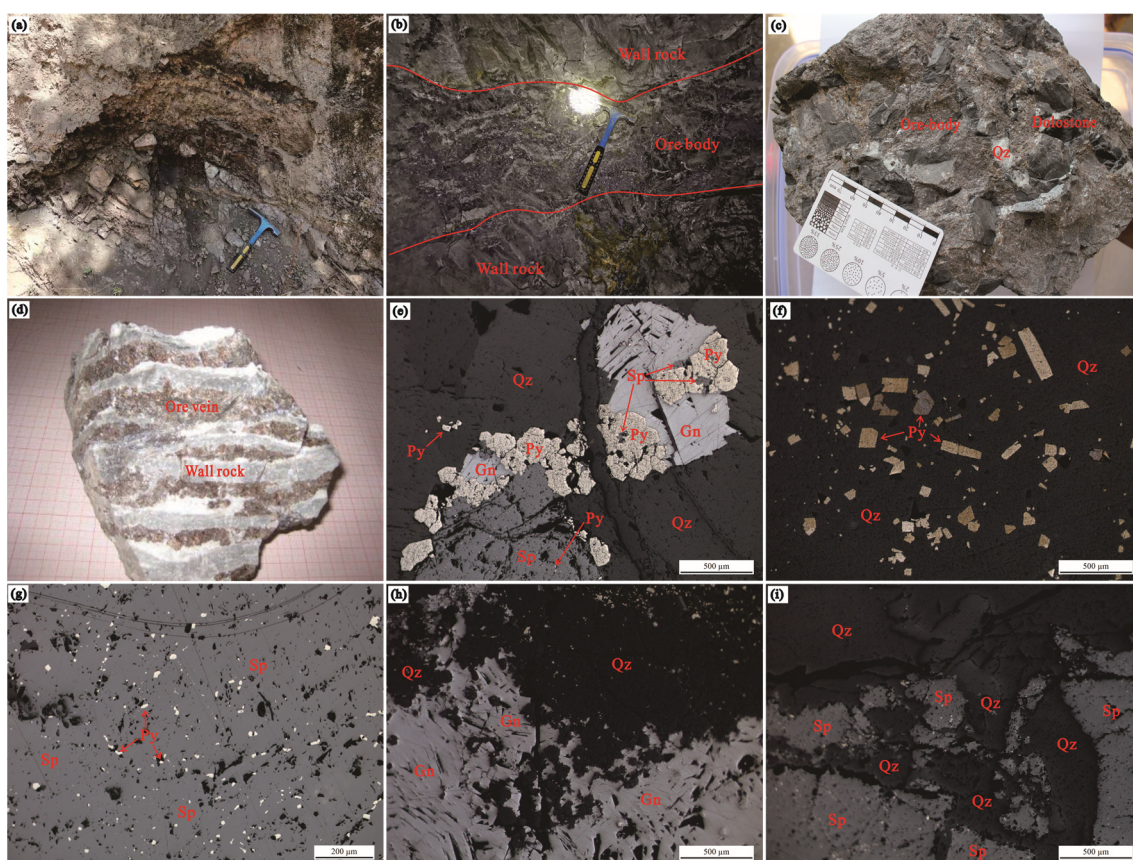
Figure 3. Ore mineralization characteristics and microscopic photos of the Maliping Pb-Zn deposit. (**a**) Interlayer sliding zone in the Maliping Pb-Zn deposit; (**b**) Stratoid ore body controlled by interlayer fault; (**c**) Brecciated ore; (**d**) Banded ore; (**e**) Pyrite and sphalerite are symbiotic, galena metasomatic pyrite and sphalerite, quartz metasomatic galena, sphalerite and pyrite; (**f**) Quartz metasomatic pyrite; (**g**) Pyrite and sphalerite are symbiotic; (**h**) Quartz metasomatic galena; (**i**) Quartz metasomatic sphalerite. (Gn = Galena; Py = Pyrite; Sp = Sphalerite; Qz = Quartz).

3. Research Methods

3.1. Sample Collection

Eight representative primary metal sulfide ores were collected from different middle sections, with six II-1 and two II-2 orebodies. Six single-mineral sphalerite and seven quartz samples were selected from among the collected samples. Seven quartz samples were analyzed for H-O isotopes, and six sphalerite samples were analyzed for trace elements and rare earth elements (REEs). We utilized eight metal sulfide ore samples and ground double-

sided polished fluid inclusion slices (thickness of approximately 200 μm). By comparing the petrography of the fluid inclusions, a microscopic thermodynamic analysis was conducted on 71 inclusions from 2 representative inclusion slices.

3.2. Analytical Methods

Single metal sulfide minerals were ground manually to 40–60 mesh, cleaned, and dried. Single minerals with a purity of over 99% were selected under binocular conditions. Subsequently, six single sphalerite minerals were crushed to less than 200 mesh in an agate mortar, and seven single quartz minerals were crushed to 60 mesh in an agate mortar for instrument analysis.

H–O isotopic testing was performed at Beijing Createch Testing Technology Co., Ltd. The hydrogen isotope testing procedures were as presented by Gong et al. [22]. The testing equipment used was a pyrolysis furnace (FlashEA, Thermo, Waltham, MA, USA) and a mass spectrometer (253 plus, Thermo, Waltham, MA, USA). The international standard material (polyethylene, IAEA-CH-7, δDV-SMOW = −100.3‰) had a test accuracy of better than 1‰ [22]. For oxygen isotope testing, the sample was ground to 200 mesh, and 6 mg of pure quartz sample was weighed. The analysis adopted the traditional BrF5 method [23] with a standard sample analysis accuracy exceeding ±0.2% and a relative standard of V-SMOW. A 253-plus gas isotope ratio mass spectrometer was used as the testing instrument.

Single-mineral trace and REE content analyses were completed at the South China Mineral Resources Supervision and Inspection Center, China. The testing instrument was an inductively coupled plasma mass spectrometer (ICP-MS), with a standard sample analysis accuracy of better than 5% and a lower detection limit of $(0.n–n) \times 10^{-9}$. The analysis and operating procedures were as presented by Qi et al. [24]. EPMA-mapping was completed at the Research Center for Analysis and Measurement, Kunming University of Science and Technology, using an EPMA-1720 with an accelerating voltage of 15 kV, current of 10 nA, and analytical accuracy of 0.01%.

Microthermometry of the inclusions and laser Raman microprobe testing of individual inclusion components were performed at the Southwest Institute of Geological Survey, Geological Survey Center for Nonferrous Metals Resources. The testing equipment used was a THMS 600 standard microscope and a Renishawin Via micro confocal laser Raman spectrometer. During microthermometry, the fluid inclusions standard sample was used to calibrate the cold and hot platform and determine the error at high (>200 °C) ± 2 °C and low temperatures (<0 °C) ± 0.1 °C. The analysis and operating procedure are shown in Goldstein and Reynolds [25]. The laser Raman microprobe test light source was 514.5 μm, with a counting time of 10 s, counting once every 1 cm^{-1} (wave number), over 100–4000 cm^{-1} all-band Qu wave peaks. The laser beam spot was 2 μm, and the spectral resolution was 2 cm^{-1}.

4. Analytical Results

4.1. Petrographic Characteristics of Fluid Inclusions

The fluid inclusions in quartz were all primary inclusions distributed in dispersed and isolated irregular shapes, such as triangular and flat. Their sizes were usually 4–10 μm, with a few were over 10 μm. The inclusions are vapor–liquid two-phase inclusions, most of which are rich in liquid-phase inclusions, with the vapor phase accounting for approximately 10%–35% (Figure 4).

#### 4.2. Microthermometry Results of Fluid Inclusions

The salinities and homogenization temperatures of 71 primary vapor–liquid two-phase inclusions in gangue mineral quartz from the metallogenic period were determined (Figure 5). The homogenization temperatures of fluid inclusions ranged from 220 to 297 °C (mean 254 °C). The salinities ranged from 5.6 to 15.7 wt% *NaCleqv* (mean 12.4 wt% *NaCleqv*).
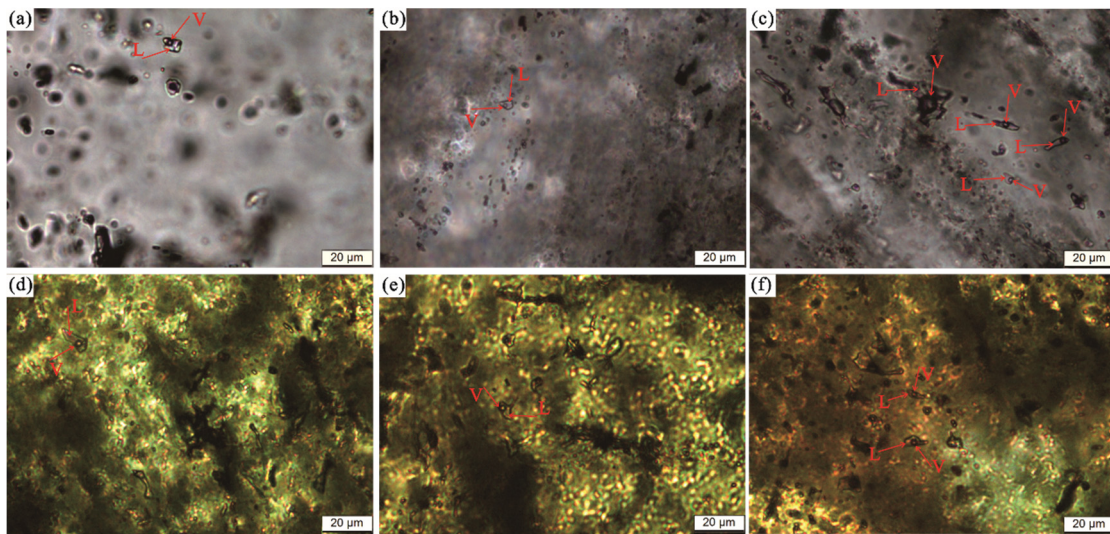
Figure 4. (**a**–**f**) Petrographic Photos of fluid inclusions in quartz of the Maliping Pb-Zn deposit. (L = Liquid, V = Vapor).
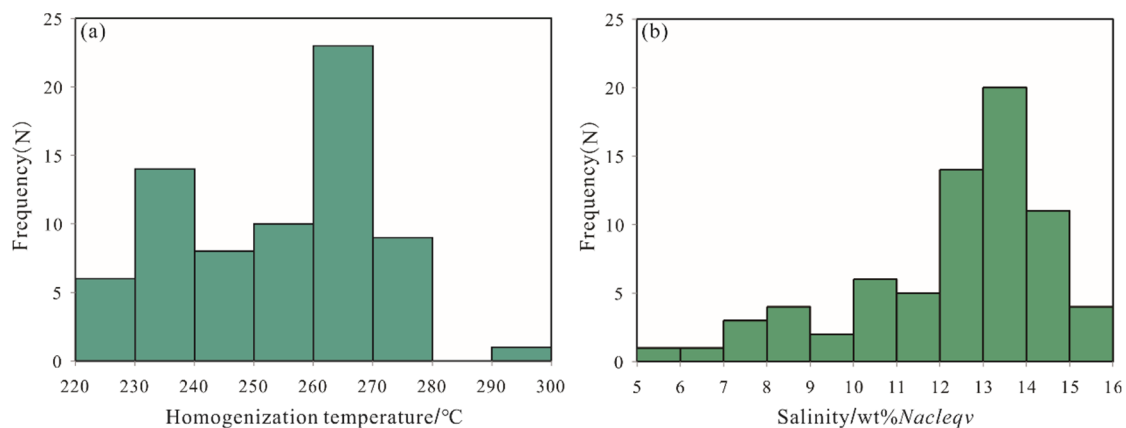
Figure 5. Histogram of homogenization temperature (**a**) and salinity (**b**) of fluid inclusions in quartz of the Maliping Pb-Zn deposit.

4.3. Laser Raman Spectroscopic Analysis

Based on microscopic laser Raman spectroscopic peak scanning of fluid inclusions (in quartz), the liquid of the measured inclusions all contain H_2O, while the vaporous parts of certain inclusions contain H_2S (2611 cm^{-1}) and N_2 (2331 cm^{-1}) (Figure 6).

4.4. Trace Elements

4.4.1. Trace Element Contents

The sphalerite is mainly dark brown and rich in various trace elements. The primary characteristics are listed as follows (Table 1).

(1) Sphalerite is rich in Cd and Cu. The content of Cd is relatively higher than that of Cu, and there is a slight variation in Cd, at 1570×10^{-6}–2160×10^{-6} (mean 1933.3×10^{-6}, n = 6). In contrast, the stability of Cu is low, with a large range of variation, at 498×10^{-6}–1860×10^{-6} (mean 925.3×10^{-6}, n = 6).

(2) Sphalerite is also relatively enriched in Pb, Sb, Hg, Ga, Ge, Ti, and Ba. The content of Pb varies greatly, at 17.7×10^{-6}–3760×10^{-6} (mean 833.6×10^{-6}, n = 6), while the contents of Ga and Ge are relatively stable, 93.8×10^{-6}–185×10^{-6} (mean 138.9×10^{-6}, n = 6) and 45.9×10^{-6}–68.8×10^{-6} (mean 57.1×10^{-6}, n = 6), respectively.

(3) The Ni, Co, As, Sn, Ag, Cr, and Mn contents are relatively low. The contents of Co and Mn are 4.77×10^{-6}–18.4×10^{-6} (mean 14.4×10^{-6}, n = 6) and 12.9×10^{-6}–73.3×10^{-6} (mean 42.1×10^{-6}, n = 6), respectively.

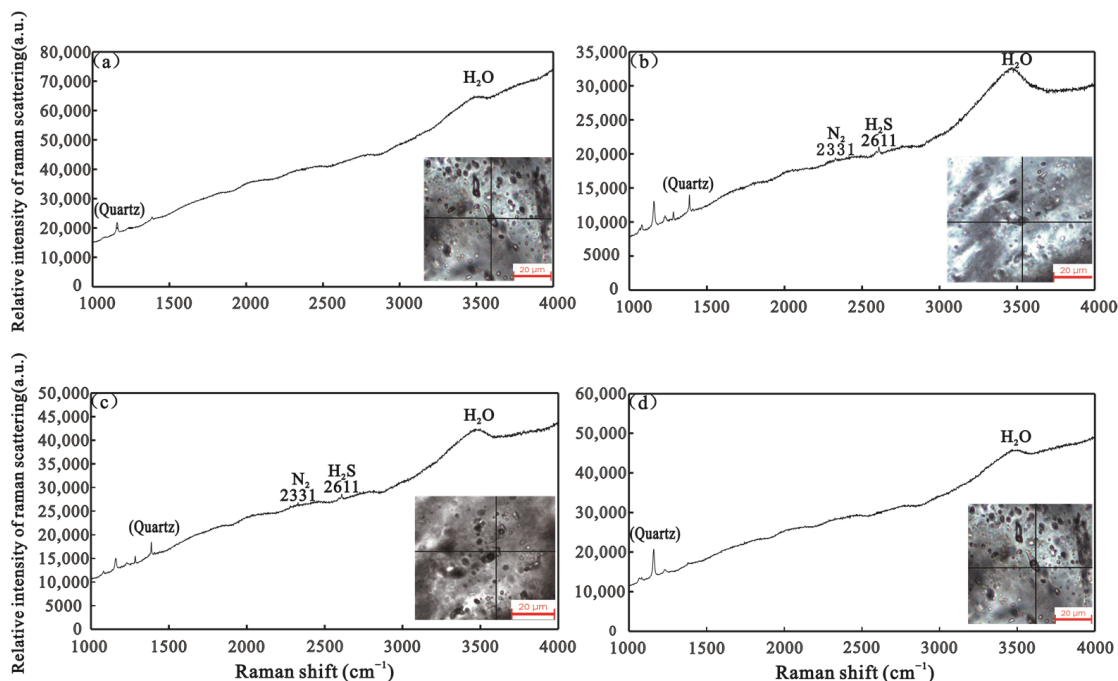(4) The contents of Li, Rb, W, Mo, Sr, Sc, Nb, Zr, Hf, Tl, U, and Th are the lowest, below 5.0×10^{-6}.

Figure 6. (**a**–**d**) Representative Raman spectra of fluid inclusions in quartz of the Maliping Pb-Zn Deposit.

Table 1. Trace element contents of sphalerite in the Maliping ore (ppm).

Element/Sample Number	MLP-1	MLP-2	MLP-3	MLP-5	MLP-6	MLP-7
Cu	498	664	868	1100	1860	562
Pb	17.7	251	755	106	3760	112
Ni	3.41	1.78	4.72	9.11	12.3	3.65
Co	14.2	18.4	16.2	17.6	15.4	4.77
Cd	1630	2070	2080	2090	2160	1570
Li	0.018	<0.01	<0.01	<0.01	<0.01	<0.01
Rb	0.6	0.75	0.67	0.73	1.96	1.24
W	0.035	0.12	0.41	0.35	1.13	3.04
Mo	0.11	0.14	0.18	0.14	2.55	0.68
As	16.1	14.3	28.9	25.3	22.7	19.6
Sb	157	305	386	411	602	295
Hg	73.9	275	198	147	212	160
Sr	0.89	1.26	12.1	1.64	3.72	2.19
Sc	0.31	0.28	0.26	0.2	0.44	0.35
Nb	<0.05	0.057	0.28	0.22	0.6	0.051
Zr	0.3	0.57	1.38	1.53	1.11	1
Hf	<0.01	0.013	0.043	0.046	0.043	0.025
Ga	97.7	142	185	154	161	93.8
Sn	12.6	33.3	31.7	37.8	18.9	5.43
Ge	60.8	45.9	55.5	52.8	58.7	68.8
Tl	0.06	0.17	0.33	0.1	0.17	0.05
Ag	6.18	20.4	44.2	16.2	44.4	17.4

Table 1. *Cont.*

Element/Sample Number	MLP-1	MLP-2	MLP-3	MLP-5	MLP-6	MLP-7
U	0.036	0.01	0.035	0.036	0.82	0.08
Th	0.098	0.095	0.14	0.082	0.4	0.23
Ti	5.01	14.7	644	361	240	18.9
Mn	12.9	73.3	60.1	40.3	52.2	14
Cr	2.77	2.99	3.57	3.84	18.08	7
Ba	6.29	49.64	77.04	27.13	504.86	47.57

4.4.2. REE Contents

The REE content and characteristic analysis results for the sphalerite are listed in Table 2. The total REE content (ΣREE) ranges from 0.24×10^{-6} to 0.78×10^{-6} (mean 0.39×10^{-6}). The light-to-heavy REE ratio (LREE/HREE) ranges from 5.67×10^{-6} to 8.48×10^{-6} (mean 6.87×10^{-6}); $(La/Yb)_N$ ($_N$ denotes the normalized value of chondrites) ranges from 9.39×10^{-6} to 27.40×10^{-6} (mean 14.97×10^{-6}); $(La/Sm)_N$ ranges from 2.33×10^{-6} to 3.47×10^{-6} (mean 2.87×10^{-6}); $(Gd/Yb)_N$ ranges from 2.38×10^{-6} to 6.29×10^{-6} (mean 3.50×10^{-6}); δ Eu (δ denotes the degree of anomaly) ranges from 1.25×10^{-6} to 2.25×10^{-6} (mean 1.84×10^{-6}), and δ Ce ranges from 0.56×10^{-6} to 0.95×10^{-6} (mean 0.71×10^{-6}).

Table 2. Characteristics of REE in sphalerite from the Maliping ore (ppm; characteristic value is dimensionless unit).

Element/Sample Number	MLP-1	MLP-3	MLP-5	MLP-6
La	0.05204519	0.15922395	0.0811368	0.11615857
Ce	0.08870712	0.21635529	0.09672696	0.11322446
Pr	0.01013269	0.03578948	0.0178416	0.0209005
Nd	0.04651827	0.17652377	0.0845352	0.09606193
Sm	0.00967212	0.04376188	0.0225144	0.02250824
Eu	0.00414519	0.03122491	0.01062	0.01487151
Gd	0.01059327	0.04116564	0.0161424	0.01969471
Tb	0.00138173	0.00600775	0.002124	0.00281353
Dy	0.00782981	0.03041702	0.0101952	0.01406765
Ho	0.00230288	0.00644108	0.002124	0.00361739
Er	0.00644808	0.01681144	0.0033984	0.00683286
Tm	0.00046058	0.00216661	0.0004248	0.00080387
Yb	0.00368462	0.01216241	0.002124	0.00643092
Lu	0.00046058	0.00173329	0.0004248	0.00080387
Y	0.05158462	0.23143821	0.0458784	0.07877882
ΣREE	0.24	0.78	0.35	0.44
LREE	0.21	0.66	0.31	0.38
HREE	0.03	0.12	0.04	0.06
LREE/HREE	6.37	5.67	8.48	6.97
$(La/Yb)_N$	10.13	9.39	27.4	12.96
$(La/Sm)_N$	3.47	2.35	2.33	3.33
$(Gd/Yb)_N$	2.38	2.8	6.29	2.53
δEu	1.25	2.25	1.7	2.16
δCe	0.95	0.7	0.62	0.56

4.5. H and O Isotopes

The H and O isotope analysis results for quartz are listed in Table 3. The $\delta^{18}O_{Quartz}$‰ ranges from 14.99‰ to 19.79‰ (mean 18.21‰), and the δD‰ ranges from −98.2‰ to −57.8‰ (mean −79.10‰). By combining fluid inclusions microthermometry data with the formula of Clayton et al. [26], $1000 \ln a = \delta^{18}O_{Quartz} - \delta^{18}O_{H2O} = 3.38 \times 10^6 \, T^{-2} - 3.4$ [T = (254 + 273.15) °C], the $\delta^{18}O_{H2O}$ in ore-forming fluids was found to range from 6.23 to 11.03‰ (mean 9.44‰) (Table 3).

**Table 3.** H and O isotopic composition of quartz in the Maliping Pb-Zn deposit.

Sample Number	δD‰	$\delta^{18}O_{Quartz}$‰	$\delta^{18}O_{H2O}$‰
MLP-1-3	−67.4	19.79	11.03
MLP-3-3	−81.3	18.52	9.76
MLP-4-3	−73.0	18.27	9.51
MLP-5-3	−86.5	18.37	9.61
MLP-6-3	−98.2	18.23	9.47
MLP-7-3	−57.8	19.28	10.52
MLP-8-3	−89.5	14.99	6.23

4.6. EPMA-Mapping

The results of the EPMA-mapping for the sphalerite are shown in Figure 7. Pb and Fe have dense optical density clusters, with Fe having more such clusters. Zn is enriched but lacking in Pb and Fe dense optical density clusters, and Cd, Cu, Ga, Ge, and Mn are uniformly distributed in sphalerite.
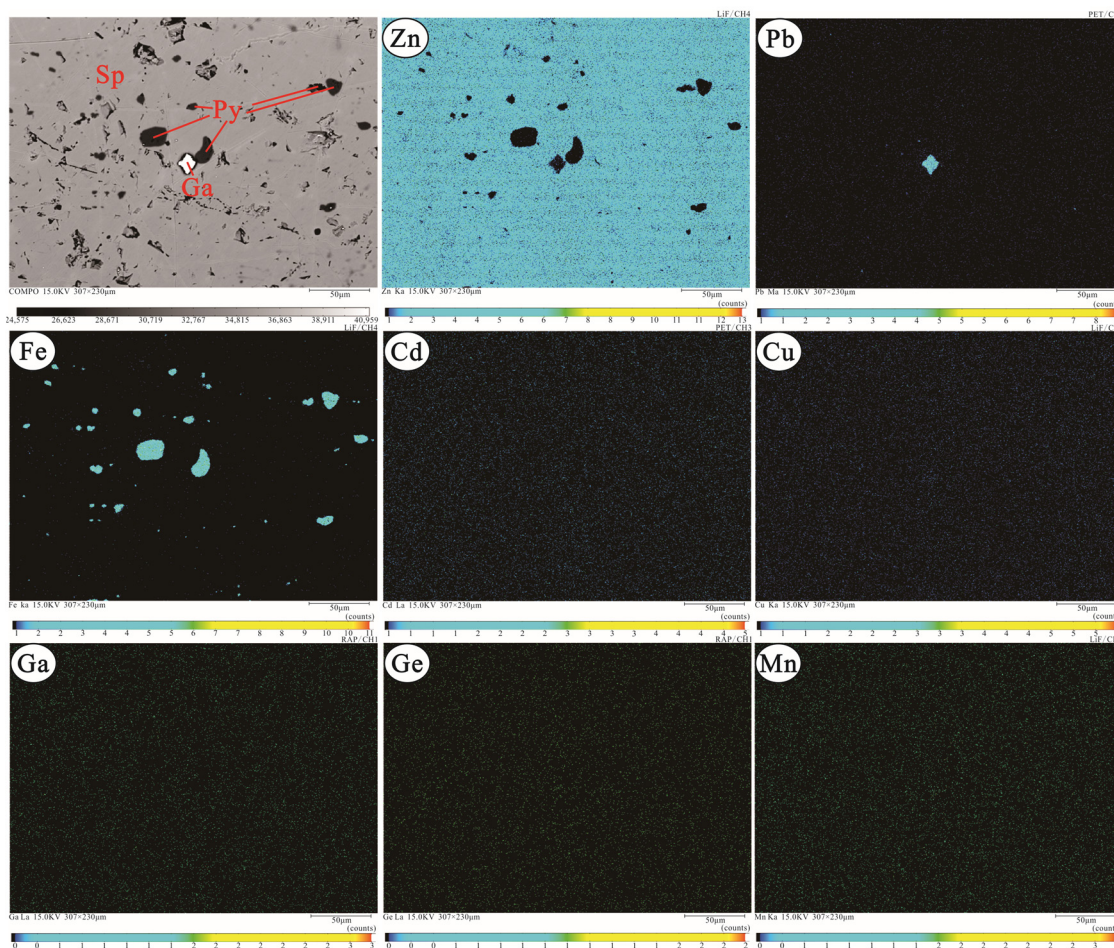
Figure 7. EPMA-mapping of sphalerite from the Maliping Pb-Zn deposit.

5. Discussion

5.1. Properties and Sources of Ore-Forming Fluids

5.1.1. Properties of Ore-Forming Fluids

(1)   Fluid density

The density of ore-forming fluids can be obtained by converting the homogenization temperature and salinity of the fluid inclusions; the density formula is [27]:

$$D = A + BT + CT^2$$

D—Fluid density (g/cm^3); T—homogenization temperature (°C); A, B, and C are dimensionless parameters, which are functions of salinity:

A = A_0 + A_1W + A_2W^2

B = B_0 + B_1W + B_2W^2

C = C_0 + C_1W + C_2W^2

W—Salinity (NaCl% weight); A_0, A_1, A_2, B_0, B_1, B_2, C_0, C_1, and C_2 are dimensionless parameters with the following values:

A_0 = 0.993531, A_1 = 8.72147 × 10^{-3}, A_2 = −2.43975 × 10^{-5}

B_0 = 7.11652 × 10^{-5}, B_1 = −5.2208 × 10^{-5}, B_2 = 1.26656 × 10^{-6}

C_0 = −3.4997 × 10^{-6}, C_1 = 2.12124 × 10^{-7}, C_2 = −4.52318 × 10^{-9}

The calculation shows that the density of ore-forming fluids in Maliping is between 0.78 and 0.95 g/cm^3 (mean 0.90 g/cm^3).

(2)　Ore-forming pressure

The ore-forming pressure estimation formula is given by P = (219 + 2620 × W) × T ÷ (374 + 920 × W) [28]

P—pressure (10^5 Pa); T—homogenization temperature (°C); W—Salinity (NaCl% weight);

The calculation shows that the pressure of the ore-forming fluids in Maliping is between 60 and 81 MPa (mean 70 MPa).

(3)　Ore-forming depth

H = P × 10^{-5}/300 [28]

H—ore-forming depth (km); P—ore-forming pressure (10^5 Pa);

The calculation shows that the depth of the ore-forming fluids in Maliping is between 2.0 and 2.7 km (mean 2.3 km).

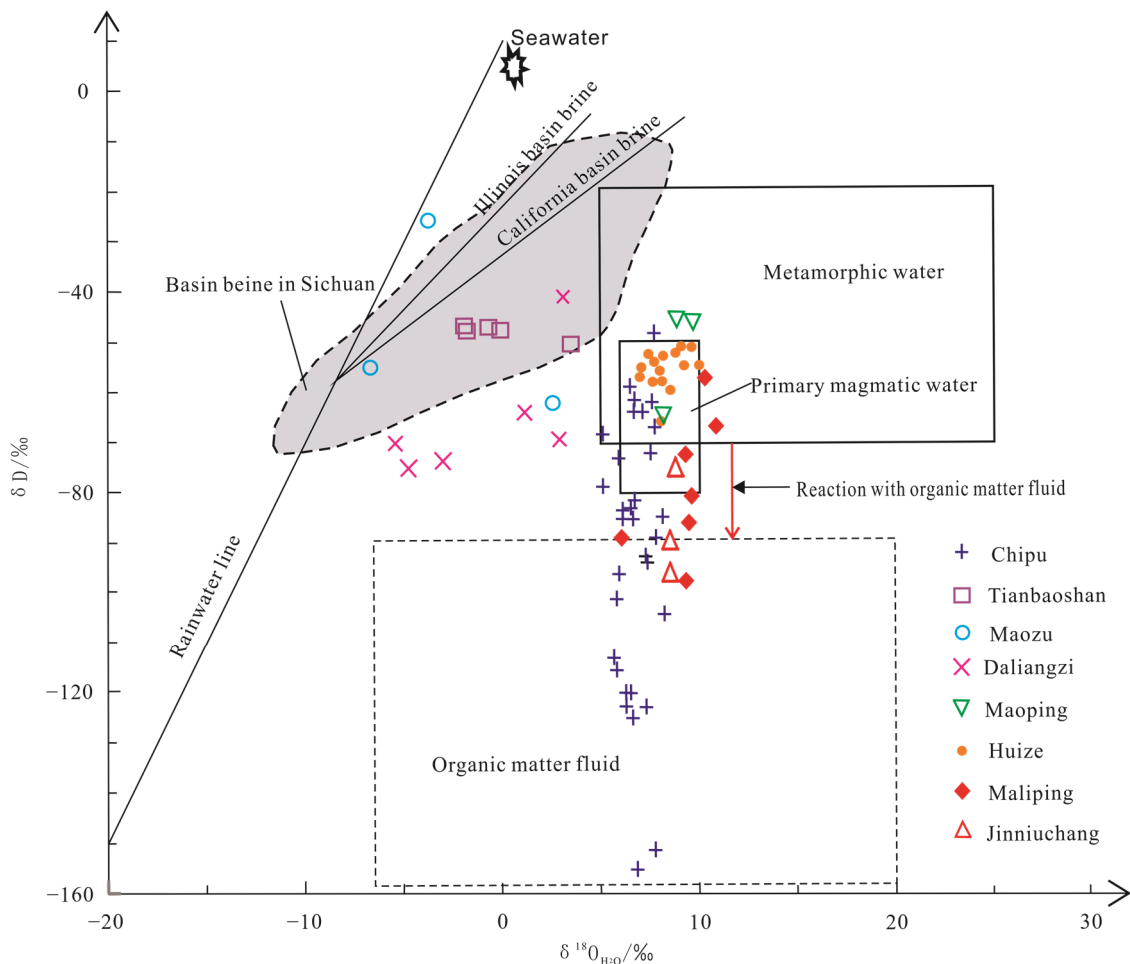### 5.1.2. Sources of Ore-Forming Fluids

In the δD-δ^{18}O$_{H2O}$ relationship diagram (Figure 8), H and O isotopes are mainly distributed among metamorphic water, primary magmatic water, and organic matter fluid, with a tendency towards organic matter fluid. However, the magmatic rocks around the ore district are mainly Emeishan basalt (approximately 260 Ma) [29–34], which is 50 Ma older than the main ore-forming age of the Pb-Zn deposits in the region (approximately 200 Ma) [35–37]. Therefore, magmatic water cannot be used as a direct source of the ore-forming fluids. Hence, the ore-forming fluids may be a mixed source of metamorphic water and organic matter fluid.

The variation range of δ^{18}O$_{H2O}$ in the deposit fluid is between 6.18‰ and 10.98‰, and the range of δD is from −98.2‰ to −57.8‰ (Table 3), indicating that the lateral drift of δ^{18}O$_{H2O}$ is not large, while the vertical drift of δD is extremely large. This pattern is similar to that of the Chipu Pb-Zn deposit, which has significant organic matter involved in mineralization [38,39]. Microscopic Raman testing results of the fluid inclusions in the deposit indicated that the vapor components were mainly H$_2$S and N$_2$, and the REE distribution pattern of the deposit exhibited negative Ce anomalies, indicating that the fluids were reducible [40]. Hence, based on the test results and comparative analysis, the ore-forming fluids have reducibility; there is organic matter involved in the mineralization, and the participation of organic matter hydrogen (δD$_{H2O}$) leads to a large vertical "drift" in δD.

Compared with the basin brine of Illinois, California, and Sichuan, the ore-forming fluids of the Maliping Pb-Zn deposit exhibit lower δD and higher δ^{18}O$_{H2O}$ (Figure 8). Within the deep source of the Maliping ore district, a series of metamorphic rocks exists in the folded basement (Kunyang Group), and REE tracing analysis suggests that the deep source fluid flowing through these rocks is mixed with the organic-containing brine, resulting in lower δD. Deep source fluids react with carbonate rocks during their ascent, resulting in higher δ^{18}O$_{H2O}$.

In summary, the ore-forming fluids of the Maliping Pb-Zn deposit were mainly derived from the mixing of deep source fluids flowing through the deep folded basement (Kunyang

Group) and organic-containing basin brine. Based on the homogenization temperature and salinity test results of the fluid inclusions and the aforementioned ore-forming fluids properties, the ore-forming fluids has medium-low temperature, medium-low salinity, medium-low density, and deep source reducibility.

Figure 8. Diagram of δD-δ^{18}O$_{H2O}$ for quartz separates from the Maliping Pb-Zn deposit. (Huize [41,42]; Chipu [38]; Tianbaoshan [43,44]; Maozu [18,45]; Daliangzi [46]; Maoping [47]; Jinniuchang [48]; Base map [49]).

5.2. Sources of Ore-Forming Materials

REEs can be used to trace the sources of ore-forming materials, among which Eu and Ce anomalies can identify the ore-forming environment and indicate the sources of ore-forming fluids to a certain extent [50,51]. The vast majority of Pb-Zn deposits in the SYGT are hosted in carbonate rocks, and there is a large range of Emeishan basalt and basement rocks (e.g., the Kunyang and Huili groups). Previous scholars have fiercely debated whether these provide material sources for the ore-forming process, with the main viewpoints being: (1) they are provided by carbonate rock strata and Emeishan basalt in coordination [18,52,53]; (2) the main ore-forming elements are provided by a mixture of Mesoproterozoic basement strata and the Sinian-Carboniferous sedimentary rock strata [41,54,55]; (3) they are mainly provided by Mesoproterozoic basement rocks [21,56–59]. Thus, the sources of ore-forming materials for the Pb-Zn deposits in the area require further investigation.

Figure 9 shows that the REE distribution pattern in fresh wall rocks of the ore district are enriched LREE, depleted HREE, weak negative Ce anomalies, and medium negative Eu anomalies. These characteristics are similar to the REE distribution pattern curve in

the upper crust, indicating that the migration amount of REEs in the fresh wall rocks was extremely small, further indicating that the REEs in the fresh wall rocks contributed little to ore-forming materials [60]. The REE distribution pattern of altered wall rocks in the ore district is consistent with that of sphalerite in the Maliping deposit, with both exhibiting right-dipping positive Eu anomalies, negative Ce anomalies, and relative enrichment of LREEs, indicating a certain genetic connection. Additionally, they had similar ΣREE contents, indicating that they had similar sources. Both exhibited positive Eu anomalies, indicating that a water–rock reaction occurred during the ore-forming process [61], and a small amount of REEs in the altered wall rocks migrated and participated in the mineralization process.

The REE distribution pattern of the Emeishan Basalt is also a relatively enriched right-dipping type for LREEs, but the regional Pb-Zn ore-forming age occurred later than the Emeishan Basalt (see above), reflecting the likelihood that ore-forming materials were provided because of the activation of the Emeishan Basalt by later ore-forming fluids [55].

The REE distribution pattern of the Kunyang Group is a relatively enriched right-dipping type of LREEs, which is consistent with the sphalerite of the Maliping deposit, indicating a certain genetic connection between the two. Additionally, the higher ΣREE contents of the Kunyang Group provided favorable conditions for sourcing REEs for the ore-forming process.

The sphalerites of the Huize, Lehong, and Maliping deposits in northeastern Yunnan have similar REE distribution patterns and ΣREE contents, indicating similar sources of ore-forming materials. The ore-forming materials for the Huize Pb-Zn deposit were mainly derived from basement rocks (Kunyang Group) and cover sedimentary rocks, whereas the Emeishan basalt may provide a small amount of material for mineralization [62]. The ore-forming materials for the Lehong Pb-Zn deposit were mainly derived from Proterozoic Eon basement rocks (Kunyang Group), with a possible contribution from sedimentary strata [9,62].

In summary, the ore-forming materials for the Maliping Pb-Zn deposit were mainly derived from the basement rocks (Kunyang Group). The altered wall rocks that underwent water–rock reactions and the Emeishan basalt, which underwent fluid activation may have provided a small amount of ore-forming materials.
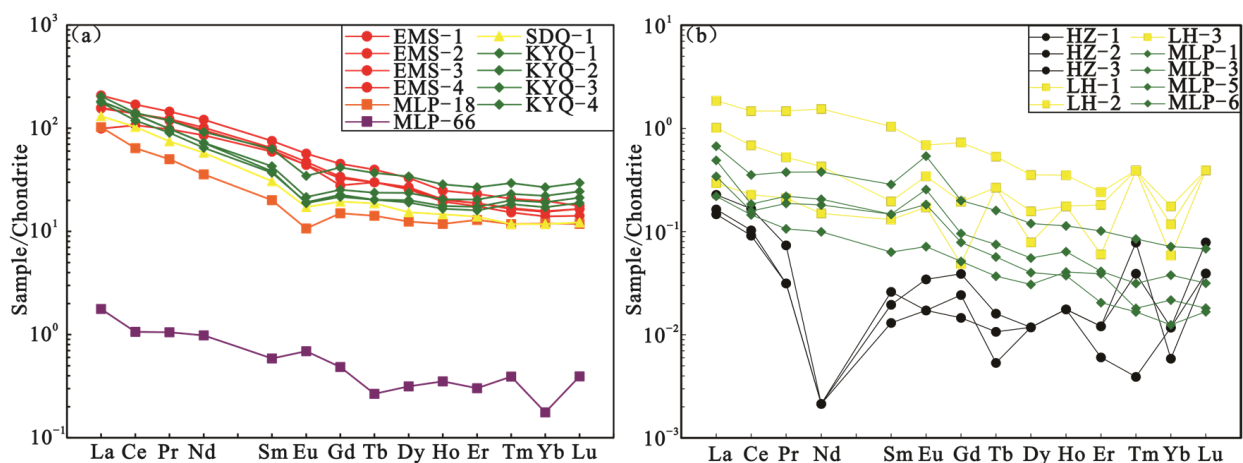
Figure 9. (**a**,**b**) Distribution pattern of REE in the Maliping Pb-Zn deposit. [(**a**): EMS-1,2,3,4 = Emeishan basalt [63]; SDQ-1 = Valuation of rare earth element abundance in the upper crust [64]; MLP-18, 66 = Fresh wall rock and altered wall rock in Maliping deposit [61]; KYQ-1, 2, 3, 4 = Metamorphic rocks of the Kunyang Group [65]; (**b**): HZ-1, 2, 3 = Sphalerite in Huize deposit [66]; LH-1, 2, 3 = Sphalerite in Lehong deposit [21]; MLP-1, 3, 5, 6 = Sphalerite in Maliping deposit].

5.3. Deposit Genesis

Trace elements of different genetic types of sphalerite have different characteristic element compositions, which can reveal the genetic type of the deposit to a certain extent [67–72]. Trace elements present in the form of isomorphic substitutions are more important typomorphic features [73]. Ye et al. [68] suggested that sphalerite in the sedimentary exhalative (SEDEX) Pb-Zn deposits in southern China are relatively rich in In, Fe, and Mn and poor in Ga, Ge, and Cd. The sphalerite in the magmatic hydrothermal Pb-Zn deposits is relatively rich in Mn, Fe, Sn, Co, and In and poor in Ga, Ge, and Cd. Most SEDEX and magmatic hydrothermal deposits contain Fe and Mn contents greater than 10% and 2000×10^{-6}, respectively. The results of the EPMA-mapping (Figure 7) showed that Cd, Cu, Ga, Ge, and Mn are uniformly distributed in sphalerite, indicating that they primarily exist in the form of isomorphism. Pb and Fe have dense optical density clusters, with Fe having a greater number of clusters, indicating that Pb and Fe exist in at least two forms—mineral inclusions (galena and pyrite) and isomorphic—within the sphalerite. Fe mainly exists in mineral inclusions of pyrite. These characteristics coincided with the corresponding trace element contents and variations (Table 1). Combining these findings, the sphalerite in the Maliping Pb-Zn deposit is found to be relatively rich in Cd, Cu, Ga, and Ge and poor in Fe, Mn, Sn, and Co, which significantly differs from the previous understanding that the deposit belonged to the SEDEX and magmatic-hydrothermal Pb-Zn deposits.

Based on significant differences in the types of ore-forming geological processes, ore-forming temperatures, ore-forming modes, genetic types of ore-bearing carbonate rocks, and exploration directions between Pb-Zn deposits in the SYGT and MVT Pb-Zn deposits, Han et al. [21] divided the carbonate-hosted non-magmatic epigenetic hydrothermal type Pb-Zn deposits into two sub-types: typical MVT and Huize type (HZT) deposits. Most carbonate-hosted non-magmatic epigenetic hydrothermal Pb-Zn deposits worldwide are intermediate transitional types between the two sub-type member deposits. Among them, HZT is an epigenetic pb-Zn deposit dominated by fluid "penetration" metasomatism and is controlled by strike-slip fault-fold structure and altered carbonate rocks. It is characterized by a high Pb-Zn grade, large deposit scale, and high metallogenic temperature (200–350 °C) [21]. By comparing trace elements in sphalerite in the Maliping, typical MVT, and typical HZT deposits (Table 4, Figure 10), the Maliping deposit was found to be rich in Cd, Cu, Ga, and Ge, similar to typical MVT and HZT deposits. However, there are also a number of differences: (i) poor Cr and Ni (Table 1), which is significantly different from the Cr-enrichment in typical HZT deposits, where the content of Cr typically exceeds 1000×10^{-6} [21], and from the relatively high content of Ni in the MVT (Upper Mississippi Valley district) deposits [74]; (ii) the Maliping deposit is hosted in the interlayer fracture zone at the interface between siliceous cataclastic dolomite and clastic rocks in the Lower Cambrian Yuhucun Formation, belonging to the interlayer detachment fracture zone and its lateral pinnate crack structural ore-control type [75], which is different from the Pb-Zn deposits hosted by carbonate rocks in typical MVT and HZT deposits.

In the Mn-Cd and Ge-Mn relationship diagrams (Figure 11), most data points of the Maliping deposit fall within the typical HZT deposit area. The content of Fe in the sphalerite (mean 6443×10^{-6}, n = 43) [16] is between HZT Pb-Zn deposits such as Huize (855.25×10^{-6}) and Maoping (21275.65×10^{-6}), and the content of Sn (mean 23.3×10^{-6}, n = 6) is slightly higher than that of Pb-Zn deposits, such as Huize (2.35×10^{-6}) and Maoping (2.78×10^{-6}) [21], implying that the Fe and Sn trace element contents in the Maliping Pb-Zn deposit are consistent with those in typical HZT deposits. The microthermometry results of the ore inclusions range from 220 to 297 °C (mean 254 °C) (slightly higher than that measured by Luo [61]), which is consistent with typical HZT deposits (200–350 °C) [21] and significantly higher than the typical MVT deposits (50–200 °C) [76,77]. The ore grade of the deposit exceeded 10%, which is significantly different from the characteristics of typical MVT deposits, where the Pb + Zn grade is usually less than 10% [21,37].

Table 4. Characteristics of some trace elements of sphalerite in the Maliping, typical MVT and HZT deposits (ppm).

Deposit Name	Deposit Type	Element	Sample Quantity	Range	Mean	Source
Upper Mississippi Valley district	Typical MVT	Mn	6	2.00~140.00	48.50	[74]
		Ag	6	2.00~46.00	21.33	
		Co	6	8.00~29.00	15.33	
		Cd	6	390.00~4000.00	1678.33	
		Cu	6	10.00~150.00	75.50	
		Ga	6	10.00~250.00	95.00	
		Ge	6	20.00~250.00	101.70	
Xiangxi Huayuan	Typical MVT	Mn	46	0.67~1305.74	132.02	[78]
		Ag	46	0.79~4.28	2.10	
		Co	38	0.00~5.03	0.50	
		Cd	46	813.00~15,964.00	7609.67	
		Cu	46	1.00~485.00	163.59	
		Ga	46	1.37~172.21	34.28	
		Ge	46	2.04~245.63	29.42	
Huize	Typical HZT	Mn	20	0.46~20.82	9.31	[21]
		Ag	20	1.39~27.39	7.06	
		Co	20	0.03~1.33	0.31	
		Cd	20	1053.97~3518.87	1881.32	
		Cu	20	7.46~319.13	137.14	
		Ga	20	0.12~65.16	11.63	
		Ge	20	3.06~231.15	80.55	
Maoping	Typical HZT	Mn	20	5.08~19.68	12.67	[21]
		Ag	20	2.29~17.10	6.76	
		Co	20	0.03~0.05	0.04	
		Cd	20	811.21~1809.66	1315.96	
		Cu	20	5.48~782.08	169.94	
		Ga	20	0.14~8.69	1.80	
		Ge	20	0.63~814.31	146.77	
Lehong	Typical HZT	Mn	9	19.13~30.86	24.19	[21]
		Ag	9	30.50~57.24	41.36	
		Co	9	0.41~41.2	7.43	
		Cd	9	1900.00~3830.00	3081.89	
		Cu	9	110.00~2480.00	658.33	
		Ga	9	9.30~158.00	51.91	
		Ge	5	11.30~59.20	34.71	
Maliping		Mn	6	12.90~73.3	42.13	This study
		Ag	6	6.18~44.40	24.80	
		Co	6	4.77~18.40	14.43	
		Cd	6	1570.00~2160.00	1933.33	
		Cu	6	498.00~1860.00	925.33	
		Ga	6	93.80~185.00	138.92	
		Ge	6	45.90~68.80	57.08	

In summary, combined with the REE distribution pattern and ore-forming material sources of the above-mentioned deposit having more similar characteristics to typical HZT deposits (Huize and Lehong Pb-Zn deposits), the genetic type of the Maliping deposit is significantly different from the SEDEX and magmatic hydrothermal types. Despite having certain similarities with typical MVT Pb-Zn and HZT Pb-Zn deposits, it is a transitional type between the two sub-type members and is more inclined to the latter. Therefore, its genetic type was defined as an HZT-like deposit.
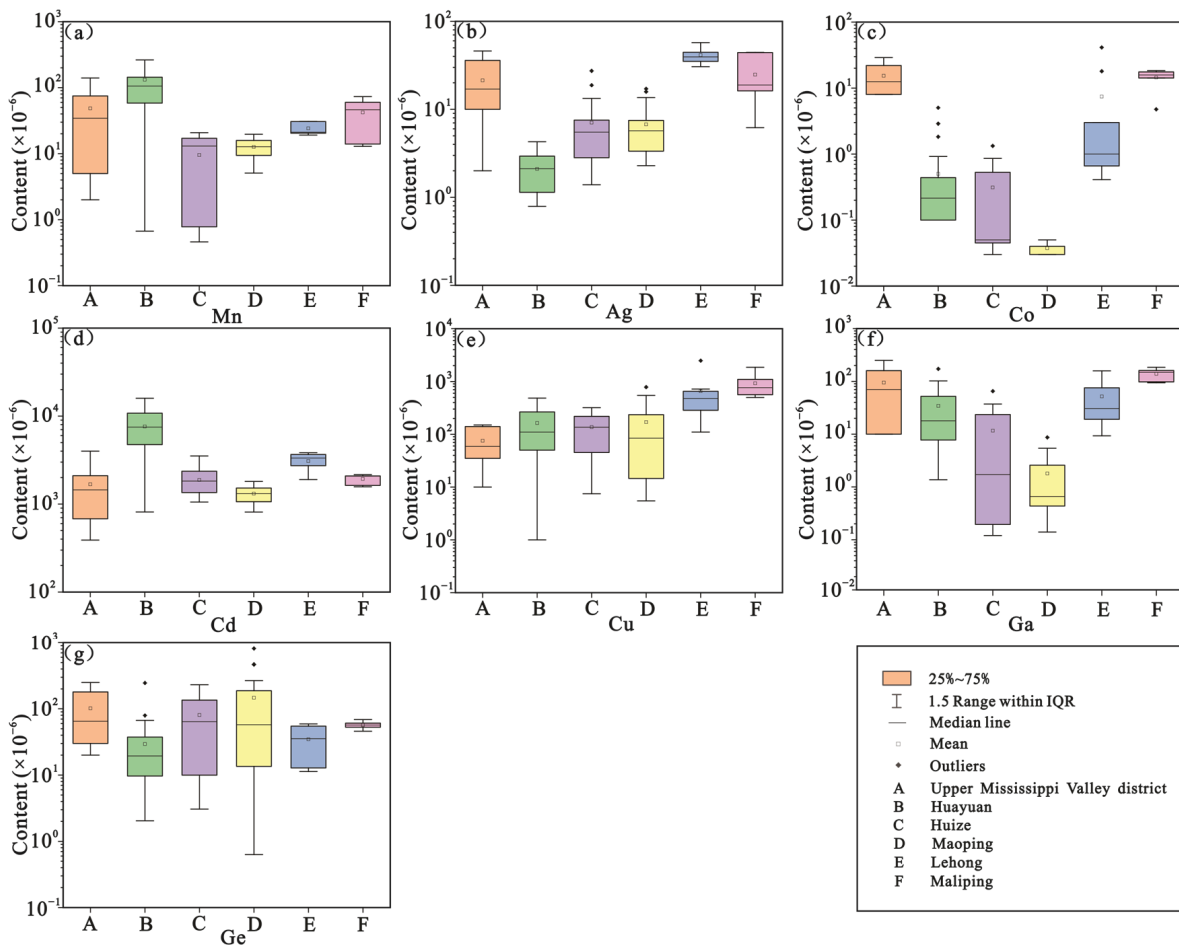
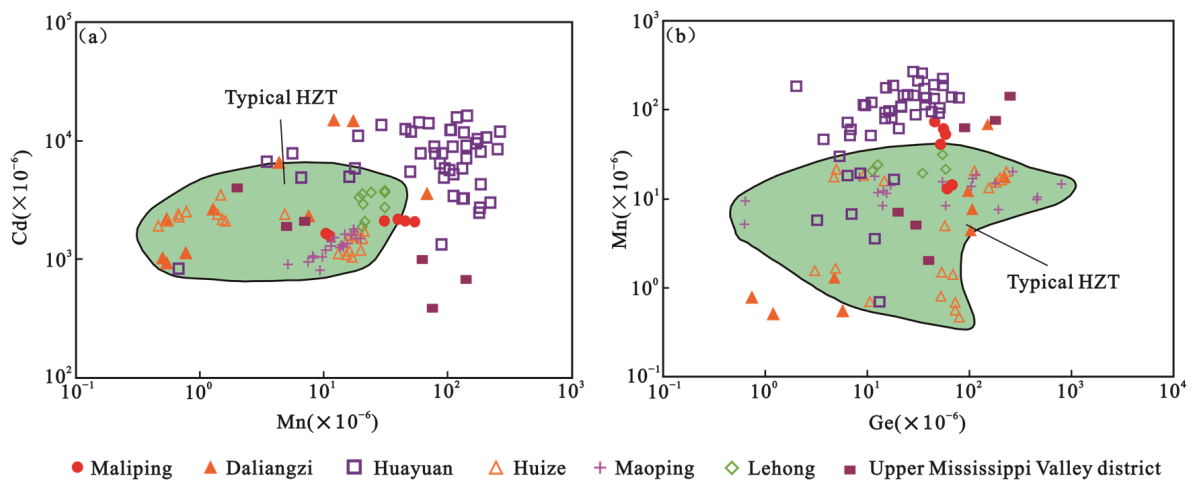**Figure 10.** (**a**–**g**) Comparison of some trace elements in sphalerite in Maliping, typical MVT and HZT deposits.

Figure 11. Relationship diagram of different types of Pb-Zn ore Mn-Cd (**a**) and Ge-Mn (**b**). (DaLiangzi [79]).

5.4. Metallogenic Mechanism and Ore Prospecting Indicative Significance

5.4.1. Metallogenic Mechanism

The genetic type of the Maliping Pb-Zn deposit was HZT-like. Considering the results of Han et al. [20] with regard to the ore-forming dynamic background of the HZT Pb-Zn deposit, Luo et al. [17] proposed that the reduced sulfur of the Maliping Pb-Zn deposit

was mainly derived from the thermal-chemical sulfate reduction (TSR) of seawater sulfate. The metallogenic mechanism of the deposit can be described as follows. During the Triassic period (230–200 Ma), the collision between the Indochina and Yangtze blocks led to the closure of the Paleo-Tethys Ocean, forming the Nanpanjiang-Youjiang orogenic belt, with regional tectonic stress conducted into the Yangtze Block, forming a series of strike-slip fault-fold structural belts in the SYGT and the Wuxing anticline. Tectonic dynamics drove high temperature and low salinity deep fluids upward along the Xiaojiang and branch faults, gradually extracting the major ore-forming metal ions such as Pb and Zn from the basement (Kunyang Group) and forming a large number of medium salinity fluids rich in ore-forming materials. In addition, under strong extrusion stress and/or orogenic uplift gravity, basin fluids containing organic matter exhibited large-scale and long-distance migration along the stratigraphic carbonate karst, gradually extracting the gypsum-salt layer sulfates in the marine carbonate rocks of the Lower Cambrian Yuhucun Formation and forming a medium-high salinity acidic fluid containing SO_4^{2-}. When the two fluids migrated to the tensile space of the interlayer detachment fracture zone of the Lower Cambrian Yuhucun Formation in the SE limb of the Wuxing anticline, they mixed and experienced homogenization. Simultaneously, the ore-forming fluid dissolved the carbonate rock to expand the ore-bearing space. The thermal energy brought by extensive hydrothermal flow and circulation initiated the TSR process, converting SO_4^{2-} into H_2S. With changes in physical, chemical, etc., ore-forming conditions, metal sulfides precipitated in a reducing environment to form the large-scale Maliping Pb-Zn deposit.

5.4.2. Ore Prospecting Indicative Significance

Han et al. [21] proposed a large-scale "four step style" deep ore prospecting method ((i) using deposit models to optimize ore prospecting direction; (ii) predicting favorable zones through tectonic-altered lithofacies; (iii) delineation of key target areas through structural geochemical exploration; (iv) applying geophysical prospecting technology to locate concealed ore body), which successfully combined the deposit model and ore prospecting exploration technology and achieved significant demonstration results in deep and peripheral ore prospecting on the Huize and Maoping Pb-Zn deposits in northeastern Yunnan. This study determined that the genetic type of the Maliping Pb-Zn deposit is HZT-like and constructed a metallogenic mechanism for the deposit. Thus, we can modify the "four step style" deep ore prospecting method and establish the exploration technical methods that are conformed to the actual ore prospecting of the deposit, thereby further delineating key ore prospecting target areas at the deep and peripheral areas of the deposit.

6. Conclusions

(1) The ore-forming fluids of the Maliping Pb-Zn deposit were a medium-low temperature, medium-low salinity, medium-low density, and deep source reducing fluid, mainly derived from the mixing of deep source fluid flowing through the deep folded basement (Kunyang Group) and organic-containing basin brine. The ore-forming materials were mainly derived from the basement rocks (Kunyang Group).

(2) The deposit is a transitional type between two sub-type members of the typical MVT and HZT Pb-Zn deposits and is more similar to the latter. Thus, it is an HZT-like deposit, and it is suitable to use a large-scale "four step style" deep ore prospecting method to delineate the deep and peripheral ore prospecting target areas of the deposit.

References

1. Li, L.J.; Han, R.S.; Zhang, Y.; Wu, J.B.; Feng, Z.X. Trace element signatures of sphalerite in the Sichuan Daliangzi Ge-rich Pb-Zn deposit and its implications for deep ore prospecting. *Front. Earth Sci.* **2022**, *10*. [CrossRef]
2. Li, Z.L.; Ye, L.; Hu, Y.S.; Huang, Z.L. Geological significance of nickeliferous minerals in the Fule Pb-Zn deposit, Yunnan Province, China. *Acta Geochim.* **2018**, *37*, 684–690. [CrossRef]
3. Tu, G.Z.; Hu, R.Z. Characteristic features of the vast low-temperature mineralization province in Southwest China. *Chin. Sci. Bull.* **1999**, *44*, 260.
4. Tan, S.C.; Zhou, J.X.; Luo, K.; Xiang, Z.Z.; He, X.H.; Zhang, Y.H. The sources of ore-forming elements of the Maoping large-scale Pb-Zn deposit, Yunnan Province: Constrains from in-situ S and Pb isotopes. *Acta Petrol. Sin.* **2019**, *35*, 3461–3476.
5. Jian, L.; Gao, J.G.; Dao, Y.; Tan, Q.L. Wallrock Alteration and Metallogenic Stages of Pb-Zn Deposits in the Sichuan-Yunnan-Guizhou Border Area Southwest China. *Adv. Mater. Res.* **2013**, *2695*, 2120–2124. [CrossRef]
6. Ren, T.; Zhou, J.X.; Wang, D.; Yang, G.S.; Lv, C.L. Trace elemental and S-Pb isotopic geochemistry of the Fule Pb-Zn deposit, NE Yunnan Province. *Acta Petrol. Sin.* **2019**, *35*, 3493–3505.
7. Zhang, C.Q.; Wu, Y.; Hou, L.; Mao, J.W. Geodynamic setting of mineralization of Mississippi Valley-type deposits in world-class Sichuan-Yunnan-Guizhou Zn-Pb triangle, southwest China: Implications from age-dating studies in the past decade and the Sm-Nd age of Jinshachang deposit. *J. Asian Earth Sci.* **2015**, *103*, 103–114. [CrossRef]
8. Liang, X.Y.; Li, B.; Zhang, C.N.; Qin, H.K.; Li, G.; Zhang, X.Y. Mineralogical and Geochemical Characteristics of Carbonates and Their Geological Significance to the Fuli Pb-Zn Deposit, Yunnan Province. *Minerals* **2022**, *12*, 1317. [CrossRef]
9. Zhao, D.; Han, R.S.; Wang, L.; Ren, T.; Wang, J.S.; Zhang, X.P.; Cui, J.H.; Ding, J.J. Genesis of the Lehong Large Zinc–Lead Deposit in Northeastern Yunnan, China: Evidence from Geological Characteristics and C–H–O–S–Pb Isotopic Compositions. *Ore Geol. Rev.* **2021**, *135*, 104219. [CrossRef]
10. Zhu, C.W.; Wang, J.; Zhang, J.W.; Chen, X.C.; Fan, H.F.; Zhang, Y.X.; Yang, T.; Wen, H.J. Isotope geochemistry of Zn, Pb and S in the Ediacaran strata hosted Zn-Pb deposits in Southwest China. *Ore Geol. Rev.* **2020**, *117*, 103274. [CrossRef]
11. He, Z.W.; Li, B.; Wang, X.F.; Xiao, X.G.; Wan, X.; Wei, Q.X. The Origin of Carbonate Components in Carbonate Hosted Pb-Zn Deposit in the Sichuan-Yunnan-Guizhou Pb-Zn Metallogenic Province and Southwest China: Take Lekai Pb-Zn Deposit as an Example. *Minerals* **2022**, *12*, 1615. [CrossRef]
12. Zhu, C.W.; Wen, H.J.; Zhang, Y.X.; Huang, Z.L.; Cloquet, C.; Luais, B.; Yang, T. Cadmium isotopic constraints on metal sources in the Huize Zn–Pb deposit, SW China. *Geosci. Front.* **2021**, *12*, 101241. [CrossRef]
13. Shen, L.; Rao, X.H.; Wei, W.B.; Zhang, M.H.; Tao, Y.L. Geological characteristics and its genesis of Guanyingyan ore section in Maliping Pb-Zn deposit, Huize, Yunnan. *Sci. Technol. Eng.* **2014**, *14*, 149–155+172.
14. He, S.H.; Chen, X.S.; Rong, H.F. Geological characteristics and genesis of the Maliping lead-zinc deposit in Huize County, Yunnan Province. *China Min. Mag.* **2014**, *23*, 80–87.
15. Luo, K.; Zhou, J.X.; Huang, Z.L.; Cui, Y.L.; Jin, Z.G. Geochemistry and genesis of the Maliping lead-zinc deposit in Dongchuan, Yunnan. In Proceedings of the 8th National Colloquium on Mineralization Theory and Prospecting Methods, Nanchang, China, 9–12 December 2017; p. 145. (In Chinese)
16. Hu, Y.S.; Ye, L.; Huang, Z.L.; Li, Z.L.; Wei, C.; Danyushevsky, L. Distribution and existing forms of trace elements from Maliping Pb-Zn deposit in Northeastern Yunnan, China: A LA-ICPMS study. *Acta Petrol. Sin.* **2019**, *35*, 3477–3492.
17. Luo, K.; Zhou, J.X.; Huang, Z.L.; Wang, X.C.; Wilde, S.A.; Zhou, W.; Tian, L.Y. New insights into the origin of early Cambrian carbonate-hosted Pb-Zn deposits in South China: A case study of the Maliping Pb-Zn deposit. *Gondwana Res.* **2019**, *70*, 88–103. [CrossRef]
18. Liu, H.C.; Lin, W.D. *Regularity Research of Pb-Zn-Ag Ore Deposits Northeastern Yunnan*; Yunnan University Press: Kunming, China, 1999; pp. 1–468. (In Chinese)
19. Yang, Q.; Liu, W.H.; Zhang, J.; Wang, J.; Zhang, X.J. Formation of Pb–Zn deposits in the Sichuan–Yunnan–Guizhou triangle linked to the Youjiang foreland basin: Evidence from Rb–Sr age and in situ sulfur isotope analysis of the Maoping Pb–Zn deposit in northeastern Yunnan Province, southeast China. *Ore Geol. Rev.* **2019**, *107*, 780–800. [CrossRef]
20. Han, R.S.; Wang, F.; Hu, Y.Z.; Wang, X.K.; Ren, T.; Qiu, W.L.; Zhong, K.H. Metallogenic tectonic dynamics and chronology constrains on the Huize-type (HZT) Germanium-rich Silver-Zinc-Lead deposits. *Geotecton. Metallog.* **2014**, *38*, 758–771.
21. Han, R.S.; Zhang, Y.; Wang, F.; Wu, P.; Qiu, W.L.; Li, W.Y. *The Metallogenic Mechanism of the Germanium-Rich Lead-Zinc Deposit and Prediction of Concealed Ore Location in the Ore Concentration Area of Northeastern Yunnan*; Science Press: Beijing, China, 2019; pp. 1–510. (In Chinese)

22. Gong, B.; Zheng, Y.F.; Chen, R.X. An online method combining a thermal conversion elemental analyzer with isotope ratio mass spectrometry for the determination of hydrogen isotope composition and water concentration in geological samples. *Rapid Commun. Mass Spectrom. RCM* **2007**, *21*, 1386–1392. [CrossRef]

23. Clayton, R.N.; Mayeda, T.K. The use of bromine pentafluoride in the extraction of oxygen from oxides and silicates for isotopic analysis. *Geochim. Cosmochim. Acta* **1963**, *27*, 43–52. [CrossRef]

24. Qi, L.; Hu, J.; Gregoire, D.C. Determination of trace elements in granites by inductively coupled plasma mass spectrometry. *Talanta* **2000**, *51*, 507–513.

25. Goldstein, R.H.; Reynolds, T.J. *Systematics of Fluid Inclusions in Diagenetic Minerals*; Society for Sedimentary Geology: Tulsa, OK, USA, 1994; pp. 1–199.

26. Clayton, R.N.; O'Neil, J.R.; Mayeda, T.K. Oxygen isotope exchange between quartz and water. *J. Geophys. Res.* **1972**, *77*, 3057–3067. [CrossRef]

27. Liu, B.; Duan, G.X. The density and isochoric formulae for Nacl-H2O fluid inclusions (salinity $\leq$ 25 wt%) and their applications. *Acta Mineral. Sin.* **1987**, *7*, 345–352.

28. Shao, J.L.; Mei, J.M. On the study of typomorphic characteristics of mineral inclusion in the gold deposits from volcanic terrain in Zhejiang and its genetic and prospecting significance. *Mineral. Petrol.* **1986**, *6*, 103–111.

29. Zhou, M.F.; Malpas, J.; Song, X.Y.; Robinson, P.T.; Sun, M.; Kennedy, A.K.; Lesher, C.M.; Keays, R.R. A temporal link between the Emeishan large igneous province (SW China) and the end-Guadalupian mass extinction. *Earth Planet. Sci. Lett.* **2002**, *196*, 113–122. [CrossRef]

30. Meng, F.C.; Tian, Y.L.; Kerr, A.C.; Wang, W.; Wu, Z.P.; Xu, Q.; Du, Q.; Zhou, Y.Q.; Liu, J.Q. Geochemistry and petrogenesis of Late Permian basalts from the Sichuan Basin, SW China: Implications for the geodynamics of the Emeishan mantle plume. *J. Asian Earth Sci.* **2023**, *241*, 105477. [CrossRef]

31. Shellnutt, J.G.; Denyszyn, S.W.; Mundil, R. Precise age determination of mafic and felsic intrusive rocks from the Permian Emeishan large igneous province (SW China). *Gondwana Res.* **2012**, *22*, 118–126. [CrossRef]

32. Shellnutt, J.G. The Emeishan large igneous province: A synthesis. *Geosci. Front.* **2014**, *5*, 369–394. [CrossRef]

33. Ali, J.R.; Thompson, G.M.; Zhou, M.F.; Song, X.Y. Emeishan large igneous province, SW China. *Lithos* **2005**, *79*, 475–489. [CrossRef]

34. Saunders, A.D.; Jones, S.M.; Morgan, L.A.; Pierce, K.L.; Widdowson, M.; Xu, Y.G. Regional uplift associated with continental large igneous provinces: The roles of mantle plumes and the lithosphere. *Chem. Geol.* **2007**, *241*, 282–318. [CrossRef]

35. Tang, Y.Y.; Bi, X.W.; Zhou, J.X.; Liang, F.; Qi, Y.Q.; Leng, C.B.; Zhang, X.C.; Zhang, H. Rb-Sr isotopic age, S-Pb-Sr isotopic compositions and genesis of the ca. 200 Ma Yunluheba Pb-Zn deposit in NW Guizhou Province, SW China. *J. Asian Earth Sci.* **2019**, *185*, 104054. [CrossRef]

36. Bao, M.; Zhou, J.X.; Huang, Z.L.; Jin, Z.G. Dating methods for Pb-Zn deposits and chronology research progress of Sichuan-Yunnan-Guizhou Pb-Zn metallogenic province: A review. *Acta Mineral. Sin.* **2011**, *31*, 391–396.

37. Zhou, J.X.; Bai, J.H.; Huang, Z.L.; Zhu, D.; Yan, Z.F.; Lv, Z.C. Geology, isotope geochemistry and geochronology of the Jinshachang carbonate-hosted Pb–Zn deposit, southwest China. *J. Asian Earth Sci.* **2015**, *98*, 272–284. [CrossRef]

38. Wu, Y. The Age and Ore-Forming Process of MVT Deposits in the Boundary Area of Sichuan-Yunnan-Guizhou Provinces, Southwest China. Ph.D. Thesis, China University of Geosciences Beijing, Beijing, China, 2013.

39. Wu, Y.; Zhang, C.Q.; Mao, J.W.; Ouyang, H.G.; Sun, J. The genetic relationship between hydrocarbon systems and Mississippi Valley-type Zn–Pb deposits along the SW margin of Sichuan Basin, China. *Int. Geol. Rev.* **2013**, *55*, 941–957. [CrossRef]

40. Zhao, Y.Y.; Li, S.Z.; Li, D.; Guo, L.L.; Dai, L.M.; Tao, J.L. Rare earth element geochemistry of carbonate and its paleoenvironmental implications. *Geotecton. Metallog.* **2019**, *43*, 141–167.

41. Li, W.B.; Huang, Z.L.; Zhang, G. Sources of the ore metals of the Huize ore field in Yunnan Province: Constraints from Pb, S, C, H, O and Sr isotope geochemistry. *Acta Petrol. Sin.* **2006**, *22*, 2567–2580.

42. Guo, X. Mineralization and Metallogenic Pattern of Lead-Zinc Deposits in Northeast Yunnan. Ph.D. Thesis, China University of Geosciences Beijing, Beijing, China, 2011.

43. Zhou, J.X.; Gao, J.G.; Chen, D.; Liu, X.K. Ore genesis of the Tianbaoshan carbonate-hosted Pb–Zn deposit, Southwest China: Geologic and isotopic (C–H–O–S–Pb) evidence. *Int. Geol. Rev.* **2013**, *55*, 1300–1310. [CrossRef]

44. Wang, X.C. Genesis analysis of the Tianbaoshan Pb-Zn deposit. *J. Chengdu Coll. Geol.* **1992**, *19*, 10–20.

45. Que, M.Y.; Luo, A.P.; Zhang, L.S. *Upper Sinian and Lower Cambrian Stratified Lead-Zinc Deposits in Northeastern Yunnan*; Chengdu University of Science and Technology Press: Chengdu, China, 1993; pp. 1–169. (In Chinese)

46. Yang, Y.X.; Ke, C.X.; Lin, F.C. *Metallogeny of lead-Zinc Deposit the Eastern Margin of Kangdian Axis*; Sichuan Science and Technology Publishing House: Chengdu, China, 1994; pp. 1–175. (In Chinese)

47. Han, R.S.; Zou, H.J.; Hu, B.; Hu, Y.Z.; Xue, C.D. Features of fluid inclusions and sources of ore-forming fluid in the Maoping carbonate-hosted Zn-Pb-(Ag-Ge) deposit, Yunnan, China. *Acta Petrol. Sin.* **2007**, *23*, 2109–2118.

48. Gong, H.S.; Han, R.S.; Wu, P.; Ma, L.; Chen, G. Constraints of fluid inclusion and H-O-S-Pb isotope compositions on metallogenic model of Jinniuchang Pb-Zn deposit, SW China. *Chin. J. Nonferrous Met.* **2022**, *32*, 3206–3226.

49. Kesler, S.E.; Vennemann, T.W.; Frederickson, C.; Breithaupt, A.; Vazquez, R.; Furman, F.C. Hydrogen and oxygen isotope evidence for origin of MVT-forming brines, southern Appalachians. *Geochim. Cosmochim. Acta* **1997**, *61*, 1513–1523. [CrossRef]

50. Hanson, G.N. Rare earth elements in petrogenetic studies of igneous systems. *Annu. Rev. Earth Planet. Sci.* **1980**, *8*, 371–406. [CrossRef]

51. Lottermoser, B.G. Rare earth elements and hydrothermal ore formation processes. *Ore Geol. Rev.* **1992**, *7*, 25–41. [CrossRef]
52. Huang, Z.L.; Li, W.B.; Chen, J.X.; Han, R.S.; Liu, C.Q.; Xu, C.; Guan, T. Carbon and oxygen isotope constraints on mantle fluid involvement in the mineralization of the Huize super-large Pb-Zn deposits, Yunnan Province, China. *J. Geochem. Explor.* **2003**, *78*, 637–642. [CrossRef]
53. Shen, X.L.; Lin, H.H.; Zhang, B.L.; Du, Q.X. The genesis of Guanting Pb–Zn deposits in the Jianshui area, Yunnan Province, SW China: Constraints from geochronology, S isotopes and trace elements. *Mineral. Petrol.* **2021**, *116*, 47–69. [CrossRef]
54. He, Y.F.; Wu, T.; Huang, Z.L.; Ye, L.; Deng, P.; Xiang, Z.Z. Genesis of the Maoping carbonate-hosted Pb–Zn deposit, northeastern Yunnan Province, China: Evidences from geology and C–O–S–Pb isotopes. *Acta Geochim.* **2020**, *39*, 782–796. [CrossRef]
55. Zhou, J.X.; Huang, Z.L.; Zhou, M.F.; Li, X.B.; Jin, Z.G. Constraints of C–O–S–Pb isotope compositions and Rb–Sr isotopic age on the origin of the Tianqiao carbonate-hosted Pb–Zn deposit, SW China. *Ore Geol. Rev.* **2013**, *53*, 77–92. [CrossRef]
56. Bao, Z.W.; Li, Q.; Wang, C.Y. Metal source of giant Huize Zn-Pb deposit in SW China: New constraints from in situ Pb isotopic compositions of galena. *Ore Geol. Rev.* **2017**, *91*, 824–836. [CrossRef]
57. Zhou, C.X.; Wei, C.S.; Guo, J.Y.; Li, C.Y. The source of metals in the Qilinchang Zn-Pb deposit, Northeastern Yunnan, China: Pb-Sr isotope constraints. *Econ. Geol. Bull. Soc. Econ. Geol.* **2001**, *96*, 583–598. [CrossRef]
58. Zhou, J.X.; Huang, Z.L.; Yan, Z.F. The origin of the Maozu carbonate-hosted Pb-Zn deposit, southwest China: Constrained by C-O-S-Pb isotopic compositions and Sm-Nd isotopic age. *J. Asian Earth Sci.* **2013**, *73*, 39–47. [CrossRef]
59. Oyebamiji, A.; Falae, P.; Zafar, T.; Rehman, H.U.; Oguntuase, M. Genesis of the Qilinchang Pb–Zn deposit, southwestern China: Evidence from mineralogy, trace elements systematics and S–Pb isotopic characteristics of sphalerite. *Appl. Geochem.* **2023**, *148*, 105545. [CrossRef]
60. Qi, X.X.; Li, T.F.; Yu, C.L. Rare earth element and trace element Geochemistry of Shalagang antimony deposit in the southern Tibet and its tracing significance for the origin of metallogenic elements. *Geoscience* **2008**, *22*, 162–172.
61. Luo, K. Metallogenesis of Pb-Zn Deposits in the Upper Ediacaran to Lower Cambrian in the Sichuan-Yunnan-Guizhou Pb-Zn Metallogenic Province: A Case Study of the Wusihe and Maliping Deposits. Ph.D. Thesis, University of Chinese Academy of Sciences, Beijing, China, 2019.
62. Kong, Z.G.; Wu, Y.; Liang, T.; Zhang, F.; Meng, X.Y.; Lu, L. Sources of ore-forming material for Pb-Zn deposits in the Sichuan-Yunnan-Guizhou triangle area: Multiple constraints from C-H-O-S-Pb-Sr isotopic compositions. *Geol. J.* **2018**, *53*, 159–177. [CrossRef]
63. Gong, W.M. Research of Characteristics and Petrogenesis of Emeishan Basalt in Huize Area of Yunan. Master's Thesis, East China University of Technology, Nanchang, China, 2017.
64. Rudnick, R.L.; Gao, S. Composition of the continental crust. *Treatise Geochem.* **2003**, *3*, 1–64.
65. Miao, Y.; Wei, S.G.; Lü, X.C.; Song, W.T.; Wan, L.W. Geochemical characteristics and formation environment of metamorphic rocks in Etouchang formation of middle proterozoic lower Kunyang Group in Northeastern Yunnan. *Geol. Bull. China* **2020**, *39*, 1538–1548.
66. Han, R.S.; Chen, J.; Huang, Z.L.; Ma, D.Y.; Xue, C.D.; Li, Y.; Zou, H.J.; Li, B.; Hu, Y.Z.; Ma, G.S.; et al. *Dynamics of Tectonic Ore-Forming Processes and Localization-Prognosis of Concealed Orebodies—As Exemplified by the Huize Super-large Zn-Pb-(Ag-Ge) District, Yunnan*; Science Press: Beijing, China, 2006; pp. 1–200.
67. Zhang, Q. Trace elements in galena and sphalerite and their geochemical significance in distinguishing the genetic types of Pb-Zn ore deposits. *Chin. J. Geochem.* **1987**, *6*, 177–190.
68. Ye, L.; Cook, N.J.; Ciobanu, C.L.; Liu, Y.P.; Zhang, Q.; Liu, T.G.; Gao, W.; Yang, Y.L.; Danyushevskiy, L. Trace and minor elements in sphalerite from base metal deposits in South China: A LA-ICPMS study. *Ore Geol. Rev.* **2011**, *39*, 188–217. [CrossRef]
69. Cook, N.J.; Ciobanu, C.L.; Pring, A.; Skinner, W.; Danyushevsky, L.; Shimizu, M.; SainiEidukat, B.; Melcher, F. Trace and minor elements in sphalerite: A LA-ICPMS study. *Geochim. Cosmochim. Acta* **2009**, *73*, 4761–4791. [CrossRef]
70. Belissont, R.; Boiron, M.C.; Luais, B.; Cathelineau, M. LA-ICP-MS analyses of minor and trace elements and bulk Ge isotopes in zoned Ge-rich sphalerites from the Noailhac—Saint-Salvy deposit (France): Insights into incorporation mechanisms and ore deposition processes. *Geochim. Cosmochim. Acta* **2014**, *126*, 518–540. [CrossRef]
71. Frenzel, M.; Hirsch, T.; Gutzmer, J. Gallium, germanium, indium, and other trace and minor elements in sphalerite as a function of deposit type—A meta-analysis. *Ore Geol. Rev.* **2016**, *76*, 52–78. [CrossRef]
72. Mishra, B.P.; Pati, P.; Dora, M.L.; Baswani, S.R.; Meshram, T.; Shareef, M.; Pattanayak, R.S.; Suryavanshi, H.; Mishra, M.; Raza, M.A. Trace-element systematics and isotopic characteristics of sphalerite-pyrite from Volcanogenic Massive Sulfide deposits of Betul belt, Central Indian Tectonic Zone: Insight of ore genesis to exploration. *Ore Geol. Rev.* **2021**, *134*, 104149. [CrossRef]
73. Wang, R.K. *Earth and Cosmogenic Mineralogy*; Anhui Publishing House: Hefei, China, 1989; pp. 100–108. (In Chinese)
74. Hall, W.E.; Heyl, A.V. Distribution of minor elements in ore and host rock, Illinois-Kentucky fluorite district and Upper Mississippi Valley zinc-lead district. *Econ. Geol.* **1968**, *63*, 655–670. [CrossRef]
75. Gong, H.S. Structural Ore-Controlling Characteristics and Metallogenic Mechanism of Lead-Zinc Deposits Clastic Rocks-Hosted in the Dahai Mining Area, Northeast Yunnan. Ph.D. Thesis, Kunming University of Science and Technology, Kunming, China, 2022.
76. Leach, D.L.; Sangster, D.F. Mississippi valley-type lead-zinc deposits. *Geol. Assoc. Can. Spec. Pap.* **1993**, *40*, 289–314.
77. John, R. Mississippi Valley-Type Deposits. *Rocks Miner.* **2006**, *81*, 69–71.

78. Wei, H.T.; Shao, Y.J.; Ye, Z.; Zhou, H.D. Geochemical characteristics of trace elements of sphalerite from Huayuan Pb-Zn ore field, Western Hunan, China. *J. Chengdu Univ. Technol.* **2021**, *48*, 142–153.

79. Wu, Y.; Kong, Z.G.; Chen, M.H.; Zhang, C.Q.; Cao, L.; Tang, Y.J.; Yuan, X.; Zhang, P. Trace elements in sphalerites from the Mississippi Valley-type lead-zinc deposits around the margins of Yangtze Block and its geological implications: A LAICPMS study. *Acta Petrol. Sin.* **2019**, *35*, 3443–3460.